https://doi.org/10.26599/FRICT.2026.9441280

Research Article

Formation of robust graphene tribofilms on hydrogen-free amorphous carbon/boron carbide periodic nano-multilayer coatings achieving low friction

Mingfeng Li[1,2,3,†], Pengyuan Wu[2,†], Boyang Shen[2,†], Jingjing Peng[2], Yuzhen Liu[4], Dae-Eun Kim[4], Oleksiy V. Penkov[2]✉

† Mingfeng Li, Pengyuan Wu, and Boyang Shen contributed equally to this work.

[1] School of Mechanical Engineering and Intelligent Manufacturing, NingboTech University, Ningbo 315100, China

[2] ZJU-UIUC Institute, International Campus, Zhejiang University, Haining 314400, China

[3] School of Mechanical Engineering, Zhejiang University, Hangzhou 310030, China

[4] Department of Mechanical Engineering, Yonsei University, Seoul 03722, Republic of Korea

✉Corresponding author. E-mail: oleksiypenkov@intl.zju.edu.cn

Received: January 20, 2026; Revised: May 25, 2026; Accepted: June 18, 2026

Abstract: Achieving superlubricity in hydrogen-free amorphous carbon (a-C) coatings through the formation of multilayer graphene-based tribofilms via tribochemical reactions has remained a significant challenge. Here, we report the successful fabrication of H-free a-C/B_4C periodic nano-multilayer coatings (PNCs) with systematically varied modulation periods (3-8.5 nm), which achieve low friction through tribochemically induced graphene tribofilm formation. The optimal coating structure, consisting of alternating 1.5 nm a-C and 2.5 nm B_4C nanolayers (a-C1.5), demonstrated a remarkably low coefficient of friction of ~0.075 and exceptional wear resistance (~1.3×10^{-10} $mm^3/N\cdot mm$) under ambient conditions. Advanced characterization techniques, including 2D Raman mapping and high-resolution transmission electron microscopy (HRTEM), confirmed the formation of multilayer graphene structures on the counter surface and the wear track during sliding. The formation of this multilayer graphene-based tribofilm, previously reported only in hydrogenated a-C coatings, transforms asperity-dominated shearing into low-resistance interlayer sliding between graphene nanoflakes. After extending the reciprocating sliding to 60k cycles, the tribofilm persisted, even though the coating had worn out. Molecular dynamics simulations revealed that the superior tribological performance originates from enhanced elastic recovery, optimal stress distribution across nanolayers, and boron-promoted tribochemical graphitization of amorphous carbon. This discovery demonstrates that graphene-based tribofilms can be derived from H-free a-C-based coatings, opening a novel and practical strategy for achieving low friction in carbon-based protective coatings without the limitations associated with hydrogen content or

pre-constructed 2D material additives.

Keywords: Hydrogen-free amorphous carbon; Boron carbide; Periodic nano-multilayer; Graphene tribofilm; Low friction; Molecular dynamics simulation.

1 Introduction

High shear stress, contact pressure, and flash heating at sliding interfaces can induce tribochemical reactions between the contacting surfaces, leading to the formation of protective boundary tribofilms [1,2]. Recent studies indicate that the tribological performance of amorphous carbon (a-C) coatings is determined not only by their intrinsic material properties but also by the in situ formation of tribofilms at the sliding interface, which play a pivotal role in controlling friction and ultimately achieving superlubricity [3,4]. Of particular interest is the formation of graphene and graphene-like structures through tribochemically induced rehybridization of carbon bonds. For hydrogenated a-C (a-C: H), the tribochemically-induced formation of graphene nanoscrolls on the counter surface and nanocrystalline graphite on the worn surface can significantly reduce the friction of a-C: H [5–7]. The formation of graphene-based tribofilms can enhance the antifriction at the interface by transforming asperity shearing into low-resistance interlayer slippage of graphene nanosheets. Accordingly, a-C: H coatings can be modified either by doping with elements such as Si and Al, or by incorporating other 2D materials like MoS_2; under specific conditions, these modifications promote the in situ formation of graphene-based tribofilms or

heterostructures on the counter surface and the wear tracks, leading to macroscale superlubricity [8–11].

For H-free a-C-based coatings, achieving low friction or superlubricity generally requires the introduction of additives to form protective tribofilms because of the unstable sp^2–sp^3 structural transformation during friction [12]. Additives such as graphene are typically required to achieve superlubricity in H-free a-C coatings. It has been demonstrated that pre-constructed graphene and nano-diamonds can form graphene nanoscrolls on the H-free a-C counter surface, reducing contact area through incommensurate contact, thereby significantly lowering the coefficient of friction [13]. Li et al. incorporated numerous graphene nanosheets (GNC) into H-free a-C and formed a friction pair with graphite, demonstrating that macroscale, humidity-insensitive, and structurally stable superlubricity was achieved across a wide humidity range of 2-80%. The superlubricity mechanism was attributed to the low water-molecule pinning effect and to the weak oxidation susceptibility of GNC a-C [14].

As previously noted, achieving low friction or superlubricity in both a-C and a-C: H coatings is highly dependent on several critical factors. These include the structural integrity of the additives (2D materials such as graphene and MoS_2) [15], the carefully controlled experimental conditions, and the meticulous treatment of the counter surfaces. These factors may limit the practical application of a-C coatings. In recent studies, constructing periodic nano-multilayer structures, such as a-C/Co [16], a-C/Cr [17], a-C/WC [18,19], and a-C/Ti [20], has been an effective way to achieve low friction and wear. Although graphitization has been reported in the wear tracks and tribofilms

of these H-free a-C-based coatings, the amount of graphene formed is generally very limited, making its direct detection and unambiguous characterization challenging. Moreover, the resulting graphitic species are often only locally distributed and remain structurally underdeveloped [21,22], indicating that they do not form a continuous and well-organized lubricating layer at the contact interface. Consequently, their contribution to reducing the coefficient of friction and wear rate is usually limited.

Recently, the formation of multilayer graphene tribofilms on H-free a-C/B_4C periodic nano-multilayer coatings (PNCs) has only begun to be explored [23]; however, the mechanistic role of the modulation period, long-term tribofilm durability, and the atomistic origins of the superior tribological performance — particularly the boron-promoted graphitization mechanism and its dependence on a-C layer thickness — remain poorly understood. In this study, H-free a-C/B_4C PNCs with varied modulation periods were fabricated to address these open questions systematically.

2 Experimental details

2.1 Sample preparation

As illustrated in Fig. S1, a-C/B_4C periodic nano-multilayer coatings (PNCs) were fabricated via magnetron sputtering using a custom-built system in an Ar atmosphere. To ensure a distinct gas environment for each source, isolation chimneys were installed around the B_4C and graphite magnetrons. High-purity (99.99%) B_4C and graphite targets (4-inch diameter) were utilized, with DC and RF power sources employed for the deposition of a-C and B_4C, respectively. During the a-C deposition, a substrate bias voltage of 50 V (40 kHz, 75% duty cycle) was applied. The target-to-substrate distance

was fixed at 10 cm. Polished Si wafers and SUS 316 stainless steel served as substrates. Before deposition, the substrates were ultrasonically cleaned in acetone and alcohol for 20 min and subsequently subjected to a 55 W ion beam pretreatment for 60s to enhance adhesion. The base pressure was approximately 1×10^{-5}Pa, and the working pressure was maintained at 2 mTorr. A silicon interlayer was deposited before the PNC growth to improve interfacial adhesion. Before fabricating the multilayer coatings, the deposition rates of the a-C and B_4C layers were calibrated separately under the same sputtering conditions used for multilayer deposition. Specifically, single-layer a-C and B_4C coatings were first deposited for a fixed deposition time, and their thicknesses were measured to calculate the corresponding deposition rates. Based on these calibrated rates, the deposition time of each a-C and B_4C layer was determined, and the number of deposition cycles was adjusted for each modulation period to maintain a comparable total coating thickness. The total thickness of each multilayer sample was measured individually using a 3D optical profiler, confirming that all coatings were maintained within 600 ± 30 nm. To achieve this consistency, the number of deposition cycles was adjusted based on the modulation period: 135,100, 80, 62, and 47 cycles were used for modulation periods of 3, 4, 5, 6.5, and 8.5 nm, respectively. In addition, the modulation period and individual layer thicknesses were further verified by XRR fitting, and the fitted values were close to the designed layer thicknesses.

2.2 Structure characterization

High-resolution transmission electron microscopy (HRTEM; Talos F200X, Thermo Scientific) was employed to investigate the coatings' microstructure and composition,

using cross-sectional samples prepared by focused ion beam (FIB; Crossbeam 350, ZEISS). Structural characterization was performed via X-ray reflectivity (XRR; X'pert MRD XL, Malvern Panalytical). Data fitting was conducted using X-ray Calc3 software, which applies a recursive approach based on Fresnel equations, to extract layer-specific thickness, roughness, and density values. Additionally, the total coating thickness was measured using a 3D optical profiler (Filmetrics). Mechanical properties (H and E) were assessed using an Anton Paar UNHT-3 ultranano hardness tester with a Berkovich indenter (tip radius < 20 nm). Mean values and standard deviations were calculated from 20 indentations per sample.

2.3 Tribological test

Tribological tests were performed using a custom tribometer at room temperature (30–40% relative humidity). Tests were conducted using a 6 mm steel ball (GCr 15) counter surface under a 3 N load (~1.1 GPa Hertzian contact pressure) at 5 mm/s for 10,000 cycles. All tribological tests were repeated at least 3 times. Wear tracks were analyzed by Raman spectroscopy (Renishaw, 532 nm laser), and the wear rate (WR) was calculated as $WR = V / (F \times L)$ [17].

2.4 Molecular Dynamics Simulations

Molecular dynamics (MD) simulations were conducted using the LAMMPS code [24] employing the Tersoff potential to describe Si-B-C interactions. The potential parameters used (Table S1) have been verified in previous studies [25–28]. MD simulations were accelerated using the GPU package, and visualization was performed using OVITO [29]. The simulation process was carried out in two steps. First, the

deposition of carbon and boron carbide atoms was simulated. A deposited atomic model with dimensions of 21.72 nm (x), 16.29 nm (y), and 14.715 nm (z) is illustrated in Fig. S5a. The simulation model was divided into three zones: the fixed layer (0.515 nm thick), the Newtonian zone (excluding the fixed layer), and the sputtering zone (0.2 nm thick). A timestep of 0.1 fs was adopted. Energy minimization was performed via the conjugate gradient method, followed by relaxation for 50 ps at 300 K within the canonical ensemble (NVT) to ensure thermodynamic equilibrium. Atoms for deposition are introduced into a designated "sputter" region above the substrate with initial velocities corresponding to specified kinetic energies (6-10 eV), simulating a particle flux from the sputtering zone. For the a-C1.5 model, the carbon nanolayer was generated by depositing 10 C atoms per insertion interval, with each simulation cycle lasting 20 ps. This process was repeated 360 times, yielding a C layer approximately 0.7 nm thick. Subsequently, the boron carbide nanolayer was formed by depositing 3 C atoms and 12 B atoms per 20-ps cycle. After 600 repetitions, a layer thickness of 1.05 nm was achieved. These processes were iterated to generate an a-C/B_4C model comprising two periods. Finally, the system underwent a 20 ps relaxation to achieve energy stabilization. The a-C6 model was prepared similarly; however, the deposition time for the C atoms was extended by a factor of 4.

The initial a-C/B_4C models were sectioned to create multi-period structures for the scratch simulation (Fig. S5b), yielding final thicknesses of ~12 nm. Energy minimization was performed via the conjugate gradient (CG) algorithm prior to indentation to stabilize the model. A rigid virtual indenter was employed, which

simultaneously translated laterally at 0.08 nm/ps and penetrated vertically into the coating at 0.03 nm/ps from the point of initial surface contact, following a continuous ramp trajectory. The indentation depth increased progressively throughout the scratch until reaching a final depth of 3.2 nm. This simultaneous loading mode replicates the coupled normal and tangential forces present in real tribological contacts. The force exerted on each atom within the cutoff distance was calculated using the repulsive potential $F(r) = -K(r-r_0)^2$, where K=3 eV/Å^2, r is the atom-to-center distance, and r_0 is the radius of the indenter. The F(r) was set to zero where $r > r_0$. The hybridization state of each carbon atom was determined based on a coordination number criterion with a cutoff radius of 2.0 Å.

3 Results and discussion

3.1 Analysis of the structure and mechanical properties of PNCs

The H-free a-C/B_4C PNCs with different nominal modulation periods of 3, 4, 5, 6.5, and 8.5 nm were fabricated by magnetron sputtering. For all coatings, the B_4C layer thickness was maintained at 2.5 nm, and the total coating thickness was kept constant at 600 ± 30 nm. For clarity, the PNCs were denoted as a-C0.5, a-C1.5, a-C2.5, a-C4, and a-C6 based on the thickness of a-C. The modulation period and interfacial roughness of the coatings were determined using X-ray reflectivity (XRR), as shown in Fig. 1a. As the a-C layer thickness increased, the number of reflection peaks and their corresponding intensities also increased. These changes indicate an increase in the modulation period and a reduction in interlayer mixing [23]. The measured modulation periods for a-C0.5, a-C1.5, a-C2.5, a-C4, and a-C6 were 2.94, 4.03, 5.05, 6.46, and 8.46

nm, respectively. The thickness variation across all coatings was maintained within 5%, indicating that the deposition rate was highly stable. The XRR curves for single-layer a-C and B_4C coatings were also fitted to serve as reference standards. As shown in the TEM image in Fig. 1b, the specimen with a 1.5 nm a-C layer exhibited a clear nano-multilayer structure. The dark nanolayers are identified as the ~2.5 nm B_4C, while the bright nanolayers are the ~1.5 nm a-C. The thickness results are consistent with those of XRR. Furthermore, the selected-area electron diffraction pattern confirmed that the coating was fully amorphous.

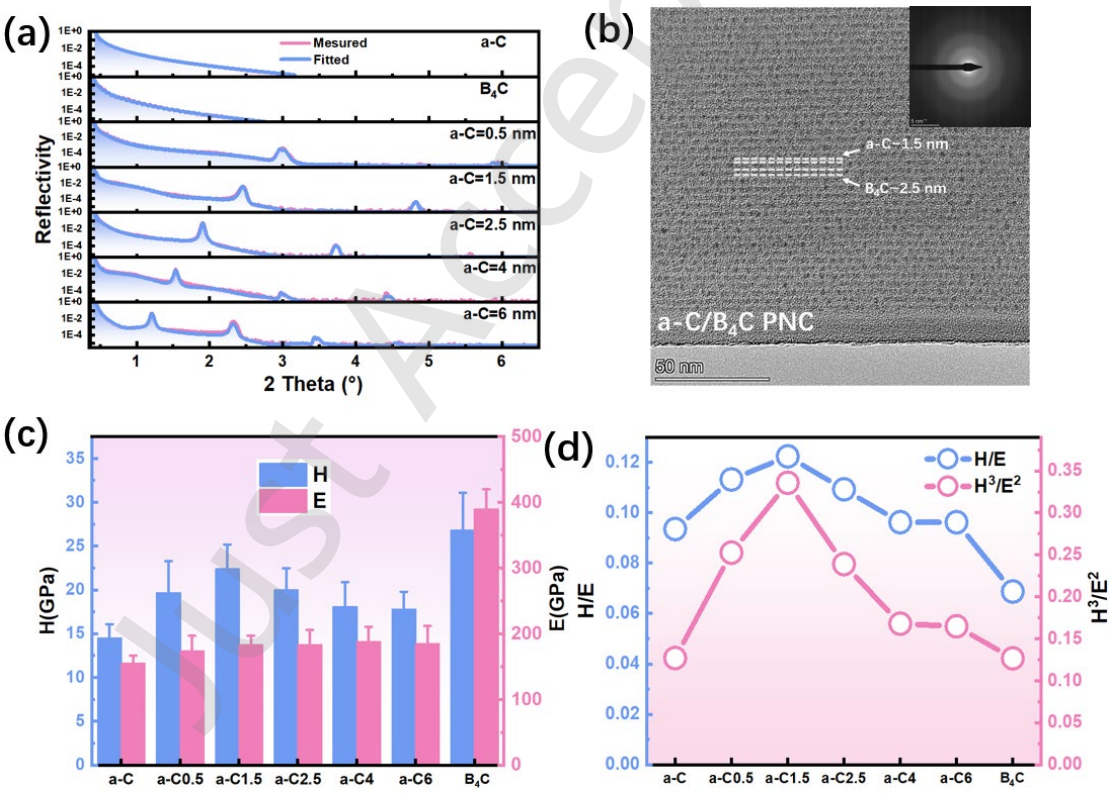

Fig. 1 Structural and mechanical characterization of the coatings. (a) Measured and fitted X-ray Reflectivity (XRR) curves; (b) representative cross-sectional Transmission Electron Microscopy (TEM) image of a-C1.5 PNC; (c) corresponding hardness (H) and elastic modulus (E); and (d) the calculated elasticity index (H/E) and plasticity index (H^3/E^2).

Fig. 1c-d presents the hardness (H) and Young's modulus (E) of the coatings, along with

the calculated H/E and H^3/E^2 ratios. Among the PNCs, a-C1.5 exhibited the highest hardness. Although the B_4C coating was harder, its H/E and H^3/E^2 ratios were significantly lower than those of the a-C1.5. The a-C1.5 presented the highest H/E and H^3/E^2 ratios, suggesting a superior elastic recovery and resistance to deformation.

Frictional curves and wear rates for each specimen are shown in Fig. 2a-b. All friction tests were conducted under the following ambient conditions: 23 °C, 45% ± 5% relative humidity, and 3 N applied load. The COF of the B_4C coating fluctuated within the range of 0.55–0.60, which is characteristic of ceramic materials [30]. In contrast, the a-C coating exhibited a relatively stable COF of approximately 0.14. Among all samples, a-C1.5 demonstrated the best tribological performance, achieving the lowest COF of ~0.075. Overall, the a-C/B_4C PNCs exhibited significantly lower COF values than the corresponding single-component coatings, indicating superior low friction. Following the friction tests, the wear volume was quantified by calculating the wear rate, as shown in Fig. 2b. The a-C1.5 PNC achieved the lowest wear rate (~1.8×10^{-10} $mm^3/N{\cdot}mm$), a value comparable to that of a-C:H coatings [31]. In contrast, the single-layer a-C and B_4C coatings showed wear rates 4 and 50 times higher, respectively, highlighting the excellent anti-wear performance of the nano-multilayer structure. The 3D wear morphology and cross-sectional depth profiles of wear tracks were shown in Supplementary Fig. S2.

3.2 Analysis of the synergistic mechanism of low friction and high wear resistance in PNCs

To elucidate the origin of the low COF of the a-C1.5 and to characterize compositional

(chemical bonding) changes in the coatings, 2D Raman mapping analysis was conducted on the tribofilms and wear tracks of all coatings. Fig. 3 and Fig. 4 showed the 2D Raman mapping of the tribofilms and the wear tracks, respectively. The severe abrasive wear observed on the ball counterfaces of the B_4C and a-C0.5 (Fig. 3a and 3b) is consistent with the morphology of their corresponding wear tracks, which are shown in Fig. 4a and 4b. Weak Raman signals for D and G peaks (I_D/I_G~2.2) were detected only at the edge of the wear scar on the B_4C counterface. On the corresponding wear track (Fig. 4a), where the B_4C coating had been mostly worn away, only a broad D peak was detected. These findings indicate that the single-layer B_4C has poor wear resistance.

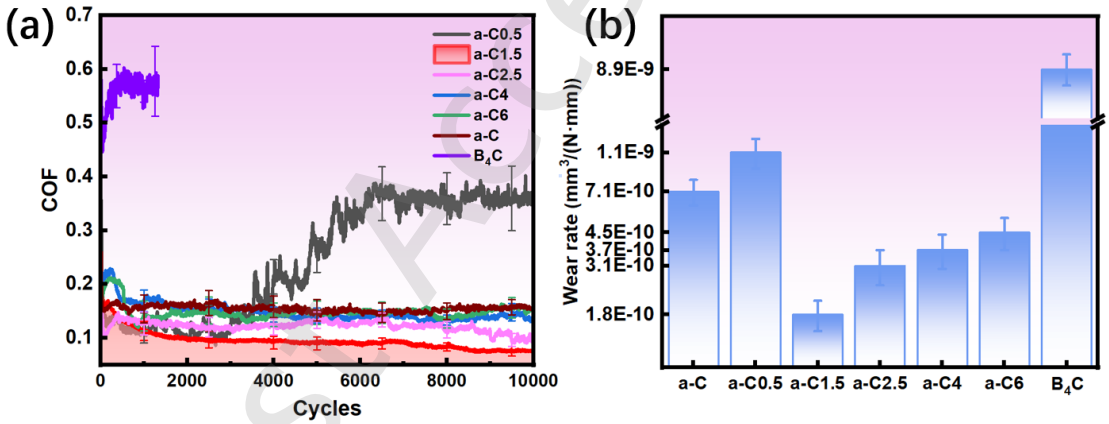

Fig. 2 Friction behavior of the coatings. (a) Coefficient of friction and (b) wear rates of the coatings.

Furthermore, the broadening of the D peak relative to the unworn surface (Supplementary Fig. S3a) suggests that B_4C underwent tribochemical reactions during sliding [32,33]. Raman analysis of the a-C0.5 sample indicated a sparse tribofilm on the counterface, as evidenced by a weak signal in the center of the wear scar despite a high I_D/I_G ratio (Fig. 3b, Point A). Since the coating was near wear-out, the similar Raman spectra observed on both the counterface and the wear track (Fig. 4b) are likely

due to a mixture of the tribofilm and the residual coating [34]. As shown in Fig. 3b, 2D Raman mapping revealed a significant deviation in the I_D/I_G ratio across the tribofilm, indicating that its distribution was highly non-uniform. Furthermore, the dominance of the B_4C phase in the a-C0.5 is the primary factor responsible for the rapid wear observed after 4000 cycles.

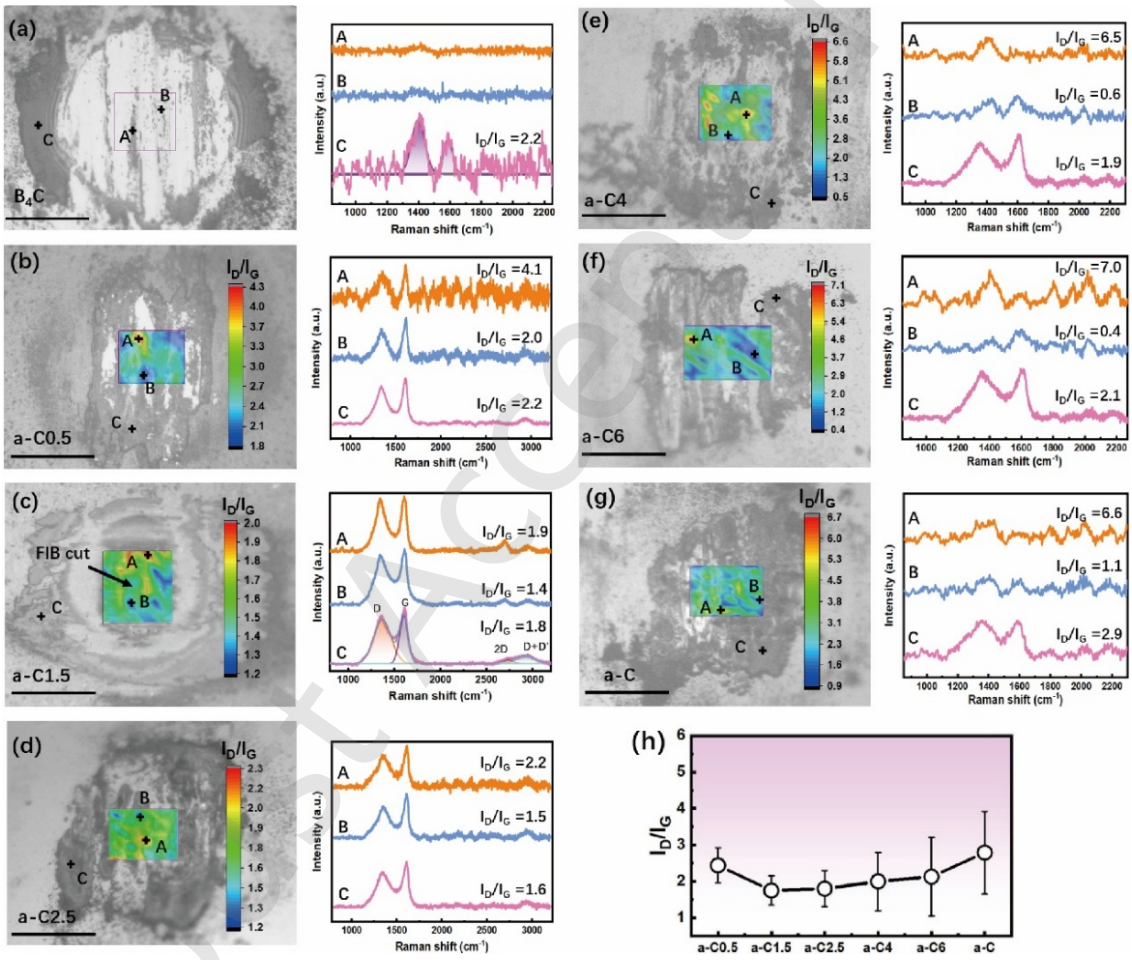

Fig. 3 Raman spectroscopic analysis of the tribofilms formed on the counter surface: (a-g) Optical images, 2D Raman maps, and their corresponding Raman spectra for each coating; (h) calculated ID/IG ratios derived from the spectra. Scale bars:100μm.

For a-C1.5, sharp D and G peaks were observed at both the center and the edge of the counter surface, along with 2D (2661 cm^{-1}) and D+D' (2929 cm^{-1}) peaks of lower intensity (Fig. 3c). The presence of 2D peaks indicates the existence of multilayer

graphene structures in the tribofilm [35]. Raman mapping demonstrates that the tribofilm is distributed with high uniformity over the counter surface. Compared with the unworn surface (Supplementary Fig. S3a), the I_D/I_G of the wear track increased significantly to 4.7 (Fig. 4c), indicating that more ordered sp^2 clusters formed [6,12,36]. Notably, in regions of the wear track where debris has accumulated, the Raman spectra reveal more pronounced 2D and D+D' peaks. A corresponding intensity ratio of the I_{2D}/I_G of 0.3 suggests the formation of multilayer graphene [37,38]. The appearance of the D + D' peak is associated with point defects in the graphene structure [38]. The observed Raman spectral features show strong similarity to those of previously reported worn graphene structures [38–40].

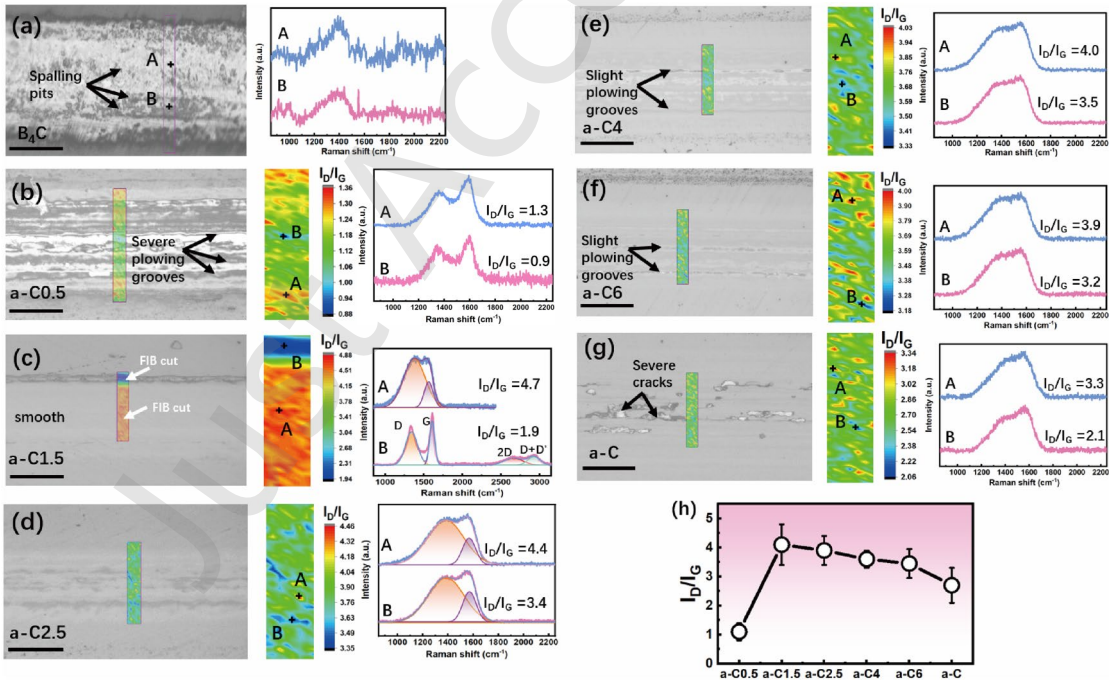

Fig. 4 Raman spectroscopic analysis of the wear tracks: (a-g) Optical images, 2D Raman maps, and their corresponding Raman spectra for each coating; (h) calculated ID/IG ratios derived from the spectra. Scale bars:100 μm.

To confirm the formation of graphene structures and reveal the low-friction mechanism of a-C1.5 PNC, samples from the debris accumulation (Fig. 4c), the region beneath the

surface of the wear track (Fig. 4c), and the counter surface (Fig. 3c) were prepared using focused ion beam (FIB) and observed via high-resolution transmission electron microscopy (HRTEM). As shown in Fig. 5a-b, a large quantity of disordered graphene lattices (d~0.33 nm) was observed in the accumulation. Among these lattices, graphitic structures were also identified, characterized by a d-spacing of ~0.22 nm, indicative of hexagonal graphite [41]. The presence of the multilayer graphene structures is attributed to tribochemical formation, as the as-deposited coating was entirely amorphous. Notably, the friction-induced graphitization described herein differs fundamentally from the mechanisms reported for hydrogen-containing a-C: H coatings. While a-C: H systems are known to reduce friction via the in situ generation of easily sheared graphene sheets or nanoscrolls at the sliding interface [6], these mechanisms cannot be directly applied to hydrogen-free a-C systems due to critical differences in hydrogen content and initial carbon bonding states. Instead, the structural transformation in this H-free system is driven by boron, which has been shown to promote the graphitization of carbonaceous materials effectively. The presence of boron reduces the activation energy necessary for the structural rearrangement of carbon atoms [42]. Additionally, boron acts as a structural template, providing nucleation sites that guide carbon atoms into ordered layers, promote a preferred orientation of the basal planes, and accelerate graphitization [43,44]. Ultimately, the localized frictional heat and shear stress generated during reciprocating sliding supply the energy required to drive this promoted transformation from amorphous carbon to multilayer graphene structures [1,45].

As presented in Fig. 5c, two distinct regions were observed beneath the wear track. The original a-C/B_4C multilayer structure was retained in the area farther from the wear

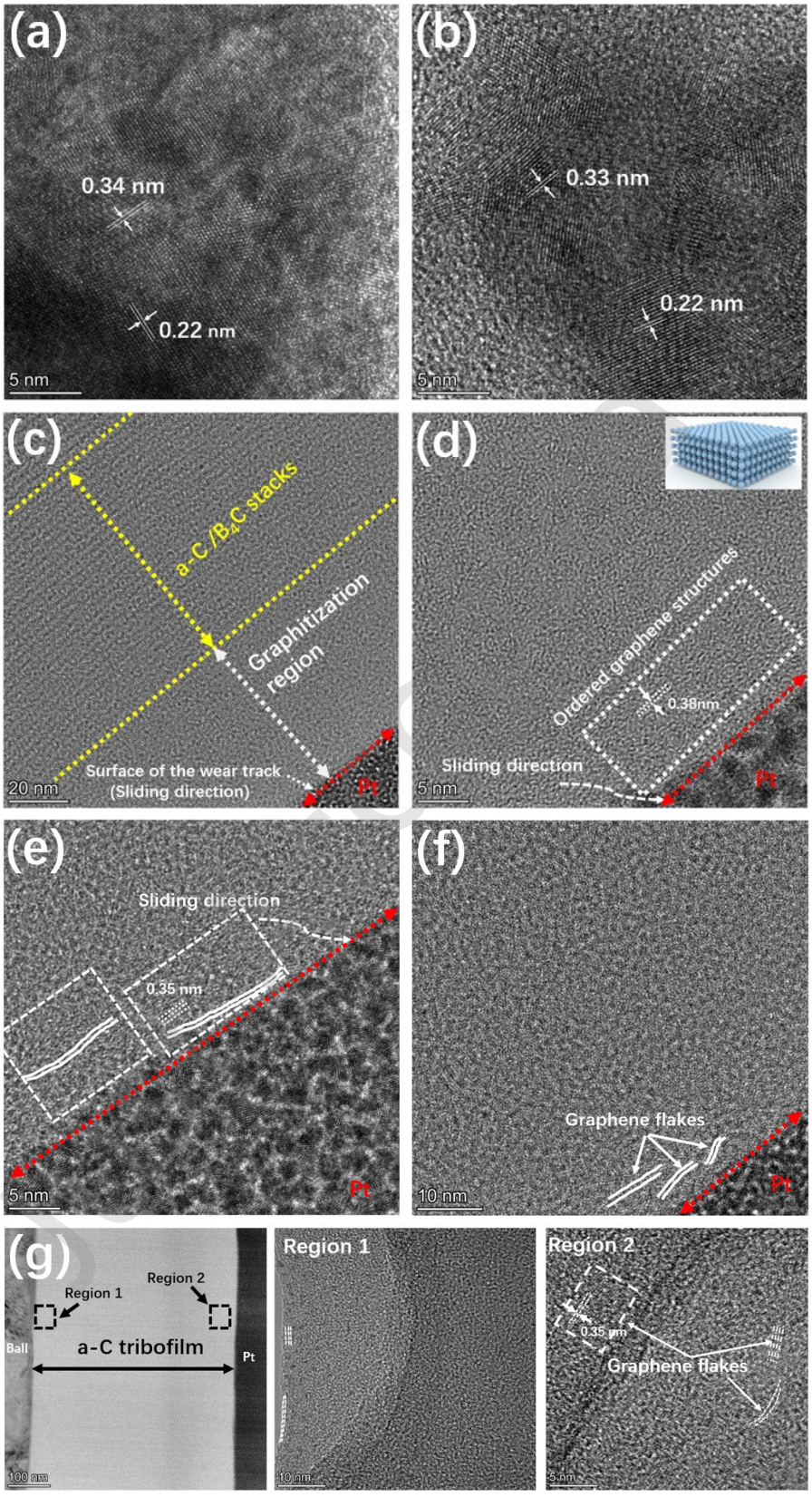

Fig. 5 HRTEM images of the a-C1.5 coating: (a-b) pile-up regions; (c-f) the worn surface ; (g) the tribofilms on the corresponding counter surface.

track, as the coating had not been completely worn away. The distinct interfaces and

consistent modulation periods indicate that this region was minimally affected by frictional shear stress. In contrast, the area adjacent to the wear track surface exhibited clearly defined and ordered multilayer graphene structures (interlayer spacing: 0.35 nm) that were preferentially aligned parallel to the sliding surface. This structural evolution indicates that continuous cyclic shear stress during reciprocating sliding induced a directional rearrangement of the carbon atoms, resulting in the formation of a highly oriented graphitic layer. Furthermore, multilayer graphene structures were rarely found beneath the wear-track surface, as shown in Fig. 5d–f. The presence of such structures within the wear track of an a-C-based coating is a notable finding, as comparable features have previously been reported exclusively in a-C: H coatings [5,7,31].

Fig. 5g displayed TEM images of the tribofilm on the counter surface. The HRTEM (Fig. 5g, Regions 1 and 2) confirmed that the tribofilm is predominantly amorphous, but also contains multilayer graphene flakes. This observation is consistent with the Raman results previously presented in Fig. 3c. Based on the preceding TEM analysis, the low-friction behavior of the a-C1.5 PNC is due to the tribochemical formation of a multilayer graphene-based tribofilm at the friction interface. Graphene is continuously transferred from the contact interface to the counter surface [2,38], forming a dense, easily sheared tribofilm. This multilayer graphene boundary tribofilm converts shear collisions at asperity contacts into interlayer slippage of graphene nanoflakes, thereby enhancing the interface's antifriction and wear resistance [46,47]. Boron plays an effective promotional role in this process, accelerating the tribochemically induced graphitization of amorphous carbon [44,48,49].

In the case of a-C2.5 PNC, optical microscopy revealed that the tribofilm is less dense than that of a-C1.5. Its Raman spectrum showed a profile similar to that of a-C1.5, but the 2D peak was absent. Furthermore, the I_D/I_G ratio of the a-C2.5 tribofilm was slightly higher than that of a-C1.5, indicating a higher sp^2 ratio and more defects in the film [34,50]. In contrast, progressive attenuation of the D and G peak signals was observed in the Raman spectra from the central contact area for the a-C4, a-C6, and a-C tribofilms (Fig. 3e-g), suggesting the formation of poorer quality and less compact tribofilms. However, strong Raman signals were detected at the edge area (Fig. 3e-g, point C), indicating an enrichment of the tribofilm and suggesting that the tribofilm was continuously squeezed out of the central contact zone and accumulated at the edge during sliding. Poor tribofilm quality is considered a primary reason for reduced wear resistance and increased friction coefficient [51]. As shown in Fig. 4e-4f, the worn surfaces of a-C4, a-C6, and a-C displayed more plowing grooves compared to those of a-C1.5 and a-C2.5. Severe cracks were observed on the worn surface of the a-C. These phenomena indicate that periodic nanomultilayers can effectively reduce and optimize stress distribution [16,52,53]; this interface-strengthening effect is known to weaken as the modulation period becomes too large [18], thereby decreasing the coating's mechanical integrity. Concurrently, the I_D/I_G ratio of the worn surfaces decreased with increasing a-C layer thickness, indicating a diminished graphitization effect, as the promotion effect of the constant-thickness boron carbide layer is less effective across thicker a-C nanolayers [42]. It is noteworthy that the I_D/I_G ratios of the tribofilms and the worn surfaces exhibit opposing trends as the a-C layer thickness increases. This

phenomenon, similar to other experimental reports [34], is attributed to the degraded tribofilm-forming ability of the a-C4 and a-C6 coatings. During sliding, this degradation leads to the formation of a less coherent tribofilm with a higher defect density, which is reflected in its elevated I_D/I_G ratio.

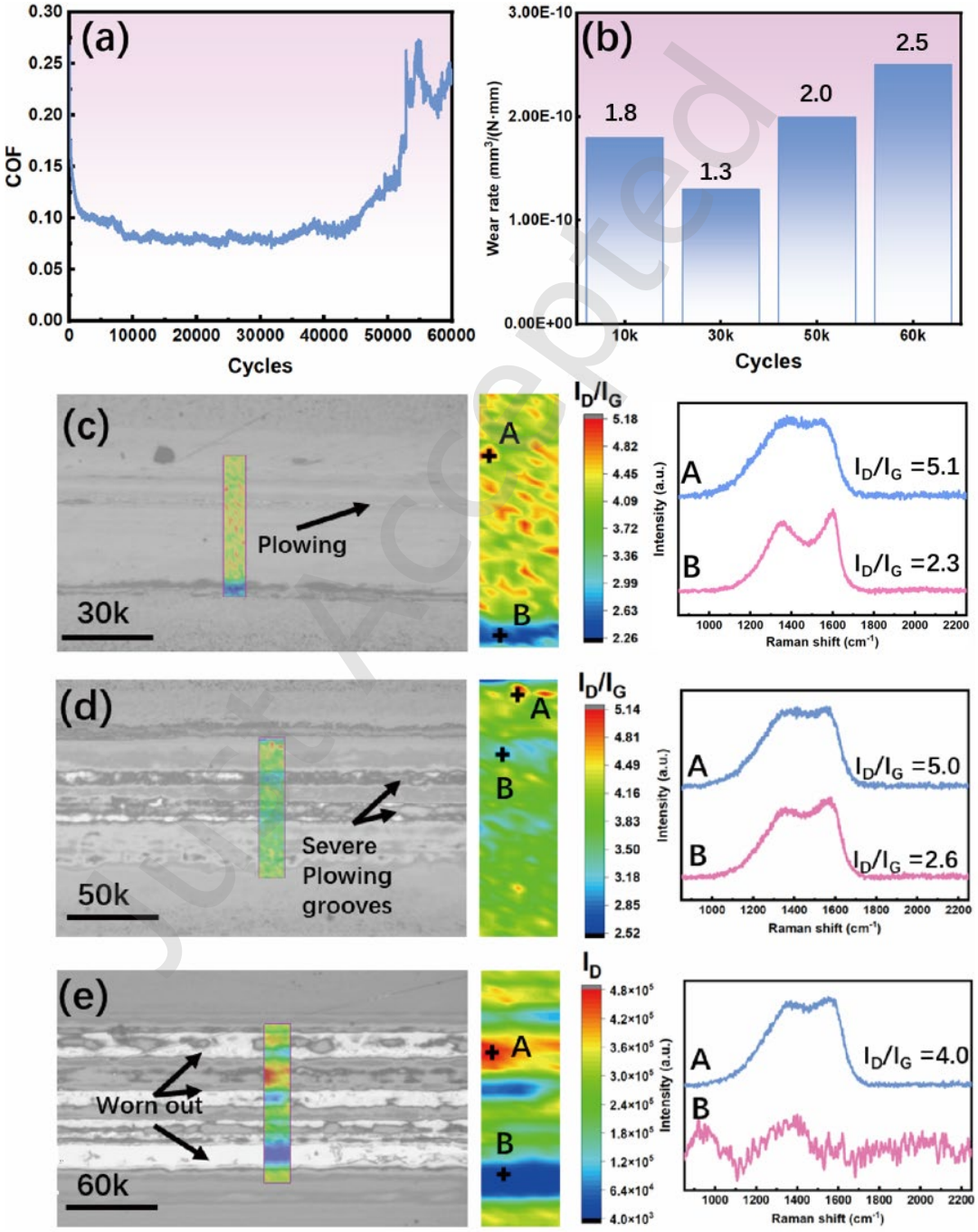

Fig. 6 Evolution of the tribofilms of a-C1.5 under 60k sliding cycles: (a) COF; (b) wear rates; and (c–e) optical images, 2D Raman maps, and corresponding Raman spectra of the wear tracks after 30k, 50k, and 60k cycles, respectively. Scale bars: 100 μm.

To evaluate the long-term durability and failure mechanism of the optimized coating, 60k extended sliding tests were conducted on a-C1.5 PNC. As shown in Fig. 6a, the coating maintained a stable, low COF of approximately 0.08 for nearly 48k cycles, after which the friction coefficient rose sharply, indicating coating failure. This transition corresponds with a progressive increase in the wear rate, which reached its maximum at 60k cycles (Fig. 6b). The evolution of the wear track morphology and chemical state is detailed in Fig. 6c–e. At 30k and 50k cycles, the wear tracks exhibited high I_D/I_G ratios (~5.0–5.1) in the central contact regions, confirming that the tribochemically induced graphitization layer persisted and provided lubrication during the stable friction phase. It is noteworthy that the wear rate reaches its minimum value (~1.3×10^{-10} $mm^3/N\cdot mm$) after 30k sliding cycles. However, at 60k cycles, the Raman signal intensity decreased significantly, with the G peak vanishing in some areas (Fig. 6e, Point B), and the spectral features of amorphous carbon disappeared, confirming that the coating had worn out. Correspondingly, the evolution of the tribofilms on the counter surface was shown in Fig. 7.

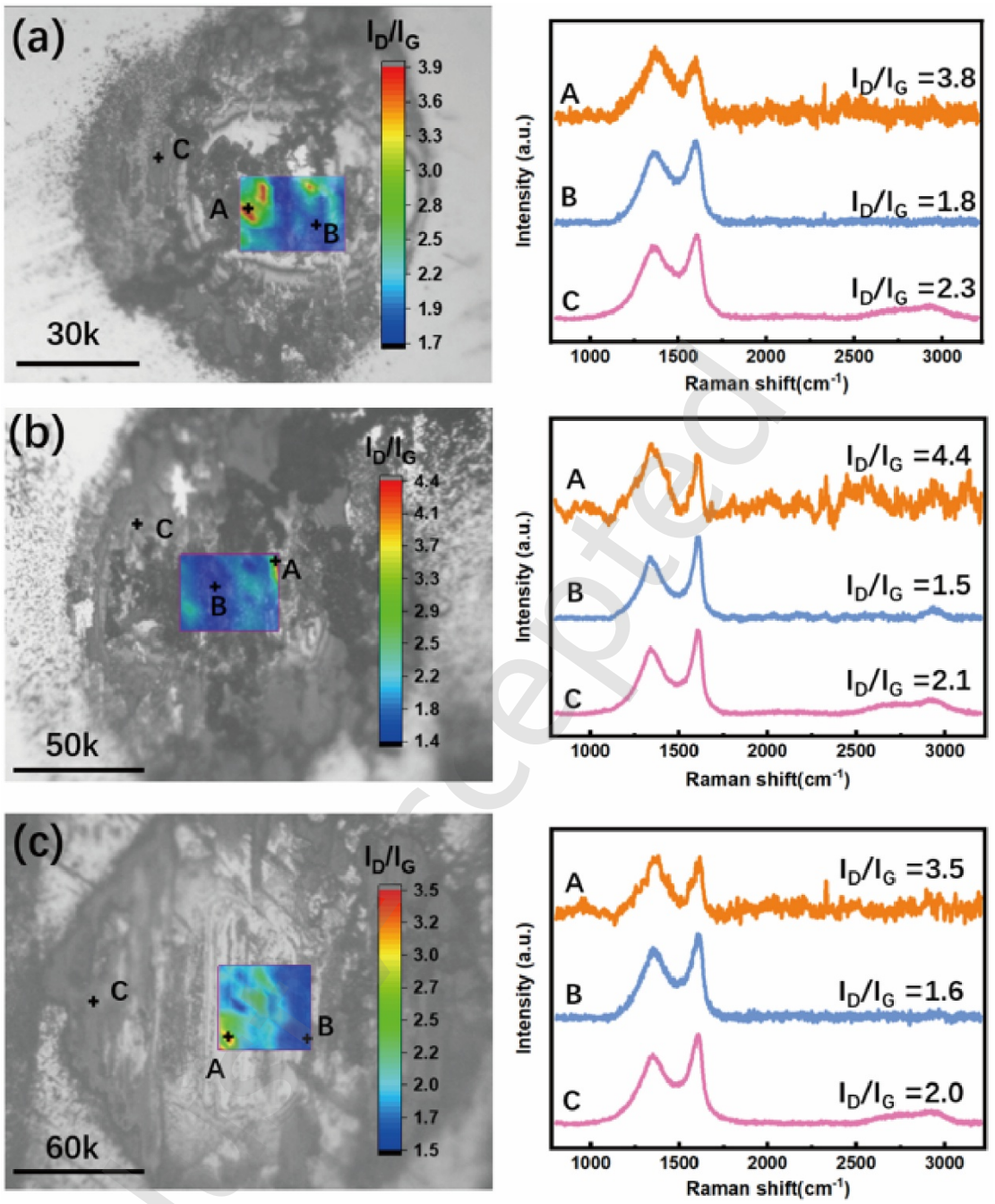

Fig. 7 Evolution of the tribofilms on the counter surface of a-C1.5 under 60k sliding cycles: (a–c) optical images, 2D Raman maps, and corresponding Raman spectra after 30k, 50k, and 60k cycles, respectively. Scale bars: 100 μm.

Throughout the stable friction period (30k and 50k cycles), a robust tribofilm was maintained on the ball surface, characterized by a lower I_D/I_G ratio in the center (~1.5–1.8) compared to the edge accumulation (~3.8–4.4). This suggests that while the contact center undergoes continuous shearing and re-ordering, the graphitized material

accumulates at the edges. Even at 60k cycles, the tribofilm remained visible with distinct D and G peaks (Fig. 7c), indicating that the tribofilm persists even as the coating is worn out. These results collectively demonstrate that the exceptional durability of the a-C1.5 PNC, with low friction over 48k cycles, can be understood in terms of a self-replenishing tribofilm mechanism enabled by the periodic multilayer architecture. During sliding, the uppermost a-C/B_4C bilayers are gradually consumed by wear, continuously exposing fresh interfaces to the frictional contact. Each newly exposed interface provides a fresh reservoir of B_4C-promoted a-C material that undergoes tribochemical graphitization under the applied contact pressure and shear stress, replenishing the multilayer graphene-based tribofilm on the counter surface. The persistent D and G peaks corroborate the regenerative process observed at 30k, 50k, and even 60k cycles in the tribofilm (Fig. 7) and the sustained high I_D/I_G ratios in the wear track (Fig. 6c–e) throughout the stable friction phase. Coating failure at ~48k cycles does not arise from the breakdown of the tribofilm formation mechanism itself — the tribofilm remains detectable even at 60k cycles — but rather from the exhaustion of the coating through abrasive wear. This self-replenishing behavior represents a distinct advantage of the periodic nanomultilayer design over single-layer a-C coatings. Although the minimum wear rate at 30k cycles is consistent with the proposed self-replenishing tribofilm mechanism, the possible contribution of graphitized debris accumulation should also be considered, as such debris may assist the formation and stabilization of graphene-based tribofilms[10]; however, work hardening of the steel counter surface is unlikely to be the dominant factor, because the wear rate increased

markedly at 50k and 60k cycles with increasing sliding cycles. Therefore, the improved wear resistance at 30k cycles is more reasonably attributed to the combined effect of debris-assisted tribofilm stabilization and the self-replenishing tribofilm process enabled by the periodic nanomultilayer architecture.

It is noted that dedicated characterization at intermediate cycle numbers (e.g., after 10k or 20k cycles) was not performed in the present study. Accordingly, the self-replenishing mechanism proposed here should be regarded as a working hypothesis that is physically consistent with the available long-duration test data, rather than a directly confirmed mechanistic description. Future work should employ systematic interrupted sliding tests at additional intermediate cycle numbers, combined with Raman mapping, cross-sectional TEM, and surface chemical analysis, to directly verify the progressive exposure of fresh a-C/B_4C interfaces and the continuous regeneration of graphene-based tribofilms.

3.3 MD Simulations of PNCs with different modulation periods

To further investigate the lubrication mechanism, molecular dynamics (MD) simulations were conducted to examine the tribological behavior of the PNCs. As shown in Fig. 8a and 8b, the periodic nano-multilayer coatings were constructed by modeling the alternating sputter deposition of C and B_4C atoms. The present MD simulations are intended to reveal relative mechanistic trends rather than to quantitatively reproduce the macroscopic reciprocating sliding experiments. Owing to

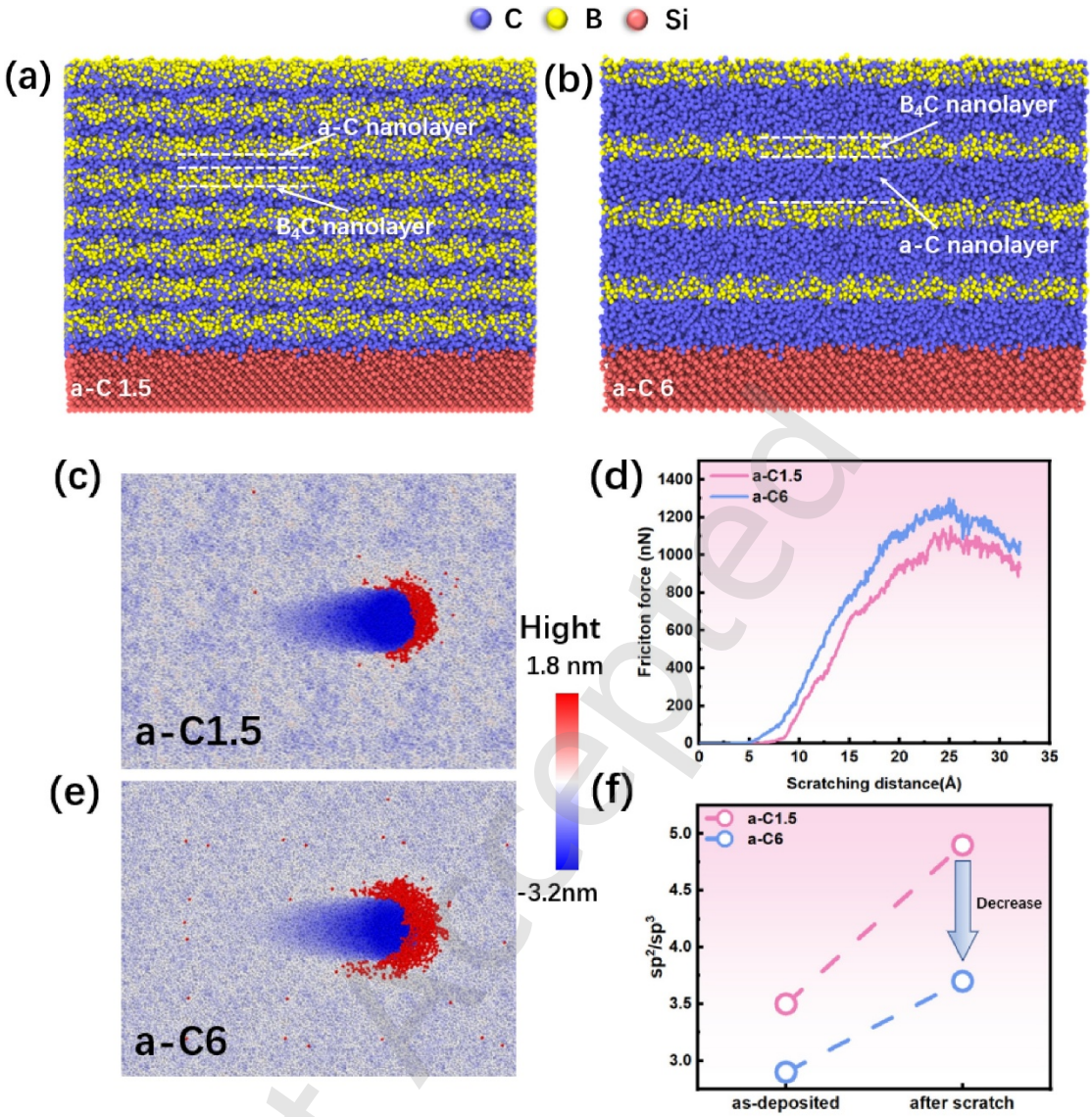

Fig. 8 Molecular dynamics simulation study (a,b) Atomistic models representing the as-deposited a-C1.5 and a-C6 coatings; (c,e) snapshots from the simulated scratch process and the resulting friction force; and (f) calculated sp^2/sp^3 ratios for the coatings before and after the scratch test.

the unavoidable differences in length scale, timescale, strain rate, and loading mode between atomistic simulations and the macroscopic tribological tests (3 N, ~1.1 GPa), the nanoscale scratch protocol should be viewed as a qualitative model of coupled normal and tangential loading. In particular, the lateral scratch velocity of 0.08 nm/ps and the vertical penetration rate of 0.03 nm/ps are much higher than the experimental sliding speed, which may accelerate bond distortion, local structural disordering, and

sp^2/sp^3 transformation compared with the experimental sliding process. Nevertheless, such elevated loading rates are inherent to conventional MD simulations because of computational timescale limitations and have been widely adopted in previous MD scratching and indentation studies as a reasonable compromise for mechanistic analysis [54,55]. Therefore, all simulation results are interpreted in terms of comparative graphitization tendency, stress distribution, and relative deformation behavior across different PNC architectures under the same nanoscale loading protocol, rather than as a direct quantitative representation of the experimental conditions.

Comparison with the HRTEM image of a-C1.5 PNC (Fig. 1b) confirmed that the simulated atomic diffusion is in good agreement with the experimental observations. Furthermore, the relatively minor edge accumulation observed at the a-C1.5 PNC indicated a higher elastic recovery capacity, which is generally associated with reduced friction [56,57]. For both a-C1.5 and a-C6, the sp^2/sp^3 ratio was observed to be higher after the scratch test than in the as-deposited state, indicating that tribochemical graphitization occurred. Previous simulations have shown that a higher sp^2/sp^3 ratio reduces friction [58]. It should be noted that the present MD framework employs the Tersoff potential, which captures B–C covalent interactions but does not resolve individual catalytic reaction pathways, such as bond-breaking activation energy reduction or nucleation-site provision—the atomic-level mechanisms through which

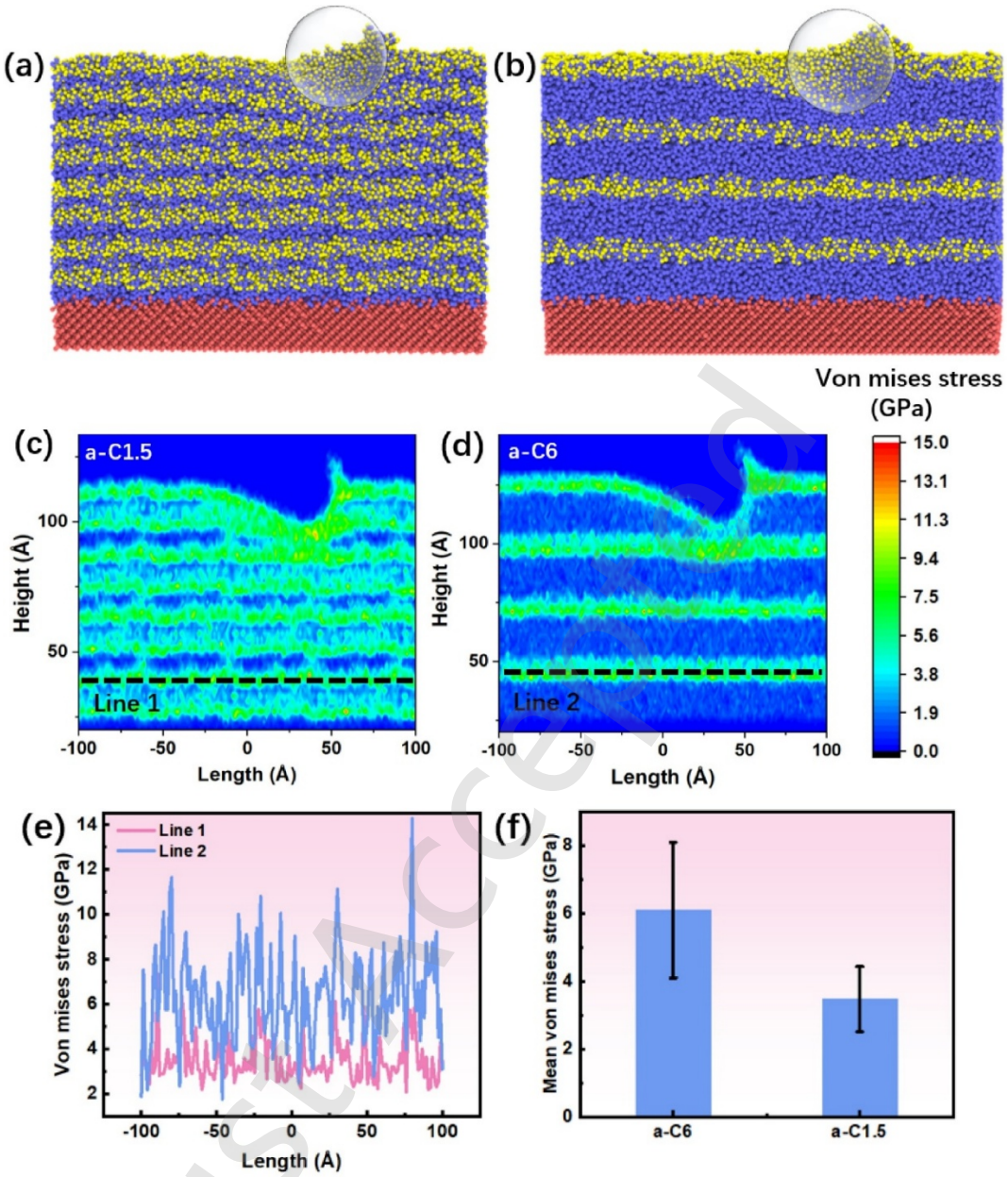

Fig. 9 Analysis of the simulated stress distribution during the scratch process: (a-b) cross-sectional snapshots of the scratch test for a-C1.5 and a-C6; (c-d) the corresponding Von Mises stress distribution maps; (e) Von Mises stress profiles extracted along Line 1 and Line 2; and (f) the calculated mean Von Mises stress for each respective line.

boron is known to promote graphitization [42–44]. The simulations, therefore, cannot directly confirm boron catalysis in the mechanistic sense. Nevertheless, the more pronounced increase in the sp^2/sp^3 ratio observed for a-C1.5 relative to a-C6 is physically consistent with a higher density of B–C interfacial contacts per unit volume, and this trend closely matches the experimentally observed I_D/I_G as a function of a-C

layer thickness (Fig. 4h). Therefore, the MD results should be interpreted as indirect atomistic support for boron-promoted graphitization rather than as direct evidence of catalytic reaction pathways. The more pronounced increase in the sp^2/sp^3 ratio in a-C1.5 compared with a-C6 is consistent with the higher density of B–C interfacial contacts per unit volume and agrees with the experimentally observed ID/IG trend as a function of a-C layer thickness.

To investigate the influence of the modulation period on scratch resistance, the stress distribution within the a-C and B_4C nanolayers was compared. Fig. 9a-b provided a schematic cross-sectional view of the scratch indentation process, while Fig. 9c-d presented the resulting post-scratch stress distribution within the coating. In the a-C1.5 coating, stress was distributed more broadly across nearly all nanolayers. In contrast, the stress in a-C6 was found to be predominantly concentrated within the B_4C layers. This indicated that the a-C1.5 coating achieved a more uniform overall stress distribution. It is noteworthy that in regions far from the scratch (Fig. 9c-d, Line 1 and Line 2), the stress magnitude within the B_4C layer of a-C1.5 is significantly lower than that in the corresponding layer of a-C6 (Fig. 9e-f). Previous studies have demonstrated that stress distribution is highly dependent on the modulation period[19]. In coatings with small periods, the high density of interfaces promotes lateral stress diffusion, leading to a more uniform distribution and preventing deep penetration[23,59]. Conversely, larger modulation periods allow stress to penetrate more deeply and become concentrated within the harder or thicker individual layers[16]. This stress concentration can subsequently induce localized plastic deformation or cracking[59].

However, if the modulation period is excessively short, residual stress can increase significantly during the deposition process [19]. This elevated stress state may, in turn, lead to premature coating failure.

4 Conclusions

In this study, H-free a-C/B_4C periodic nano-multilayer coatings (PNCs) with varying a-C layer thicknesses were fabricated, and their tribological properties were investigated. A significant discovery was made: graphene-based tribofilms can form via tribochemical reactions on H-free a-C-based coatings, a phenomenon previously thought to be confined to hydrogenated a-C coatings. The formation of multilayer graphene structures on the counter surface and in the wear track during sliding transforms the friction mechanism from asperity shearing to low-resistance interlayer slippage of graphene nanoflakes. Boron carbide plays an effective promotional role, accelerating the tribochemically induced graphitization of amorphous carbon, with promotional efficiency strongly dependent on the thickness of the a-C layer.

The superior performance of the a-C1.5 coating is attributed to a combination of enhanced mechanical properties and the formation of a protective tribofilm. The a-C1.5 sample exhibited the highest H/E and H^3/E^2 ratios, indicating excellent elastic recovery and resistance to deformation. 2D Raman analysis confirmed that this superior tribological behavior was associated with the formation of a uniform multilayer graphene structure within the tribofilm on both the counterface and the wear track. Furthermore, the periodic multilayer architecture functions as a self-replenishing reservoir of tribochemically active material: as upper bilayers are consumed by wear,

successive a-C/B_4C interfaces are exposed and continue to generate fresh graphitic tribofilm, sustaining low friction well beyond what a single-layer coating could achieve. MD simulations corroborated these experimental findings, showing that a-C1.5 underwent more pronounced tribochemical graphitization (an increase in the sp^2/sp^3 ratio) during scratching. Furthermore, the simulations indicated that the optimized 4 nm period results in a more uniform stress distribution across the nanolayers, whereas stress is concentrated in the B_4C layers.

This work presents a novel strategy for achieving low friction in hydrogen-free carbon-based coatings, eliminating the need for pre-constructed 2D material additives, controlled atmospheres, or specialized counter surface treatments, thereby expanding the practical applicability of superlubricious carbon coatings in industrial tribological systems.

Acknowledgements

This work was supported by the Zhejiang University/University of Illinois at Urbana-Champaign Institute and the National Research Foundation of Korea(NRF) grant funded by the Korea government(MSIT) (RS-2025-00560422).

Declaration of competing interest

The authors have no competing interests to declare that are relevant to the content of this article. The author Dae-Eun Kim is the Editorial Board Member of this journal.

References

[1] Berman, D, Erdemir, A. Achieving Ultralow Friction and Wear by Tribocatalysis: Enabled by In-Operando Formation of Nanocarbon Films. *ACS Nano* **15**(12): 18865–18879 (2021).

[2] Gosvami, N N, Bares, J A, Mangolini, F, Konicek, A R, Yablon, D G, Carpick, R W. Mechanisms of antiwear tribofilm growth revealed in situ by single-asperity sliding contacts. *Science* (2015) doi:10.1126/science.1258788.

[3] Liu, Y, Li, X, Xu, P, Zhang, H, Liu, L. Recent advances and challenges in tribology of diamond-like carbon films: A critical review. *Diam Relat Mater* **154**: 112206 (2025).

[4] Li, W, Chen, L, Zhang, B. A review on tribology of carbon coatings on rubber. *Friction* 1–64 (2025) doi:10.26599/FRICT.2025.9441176.

[5] Manimunda, P, Al-Azizi, A, Kim, S H, Chromik, R R. Shear-Induced Structural Changes and Origin of Ultralow Friction of Hydrogenated Diamond-like Carbon (DLC) in Dry Environment. *ACS Appl Mater Interfaces* **9**(19): 16704–16714 (2017).

[6] Gong, Z, Shi, J, Zhang, B, Zhang, J. Graphene nano scrolls responding to superlow friction of amorphous carbon. *Carbon* **116**: 310–317 (2017).

[7] Liu, Y, Chen, L, Jiang, B, Liu, Y, Zhang, B, Xiao, C, Zhang, J, Qian, L. Origin of low friction in hydrogenated diamond-like carbon films due to graphene nanoscroll formation depending on sliding mode: Unidirection and reciprocation. *Carbon* **173**: 696–704 (2021).

[8] Nadeem, I, Finšgar, M, Dražić, G, Ambrožič, B, Malok, M, Cavaleiro, A, Kalin, M. Macroscale Superlubricity with a High Load-Carrying Capacity Enabled by Nitrogen-Doped Graphene Quantum Dots in Lubricated Silicon-Doped Amorphous Carbon Films. *Small Struct* **6**(7): 2400671 (2025).

[9] Li, R, Yang, X, Zhao, J, Yue, C, Wang, Y, Li, J, Meyer, E, Zhang, J, Shi, Y. Operando Formation of Van der Waals Heterostructures for Achieving Macroscale Superlubricity on Engineering Rough and Worn Surfaces. *Adv Funct Mater* **32**(18): 2111365 (2022).

[10] Ma, Q, Fu, Y, Xu, Y, Ma, T. Achieving superlubricity and high adhesion strength of hydrogenated amorphous carbon film with Al/Cr/Si-doping. *Carbon* **215**: 118424 (2023).

[11] Sun, K, Sun, M, Chen, C, Chen, S, Fan, J, Diao, D. Structural and tribological behaviours of silicon doped amorphous carbon films. *Carbon* **215**: 118434 (2023).

[12] Chen, Z, Xing, X, Zhang, T, Zhang, S, Yang, Q, Zhang, B, Gao, K, Zhou, Y. Friction-induced metastable transformation of amorphous carbon film: Exploration by experimental and molecular dynamics simulations. *Appl Surf Sci* **628**: 157327 (2023).

[13] Berman, D, Deshmukh, S A, Sankaranarayanan, S K R S, Erdemir, A, Sumant, A V. Macroscale superlubricity enabled by graphene nanoscroll formation. *Science* **348**(6239): 1118–1122 (2015).

[14] Li, R, Yang, X, Li, J, Wang, Y, Ma, M. Macroscale, humidity-insensitive, and stable structural superlubricity achieved with hydrogen-free graphene nanoflakes. *Nat Commun* **15**(1): 9197 (2024).

[15] Berman, D, Erdemir, A, Sumant, A V. Approaches for Achieving Superlubricity in Two-Dimensional Materials. *ACS Nano* **12**(3): 2122–2137 (2018).

[16] Penkov, O V, Devizenko, A Yu, Khadem, M, Zubarev, E N, Kondratenko, V V, Kim, D-E. Toward Zero Micro/Macro-Scale Wear Using Periodic Nano-Layered Coatings. *ACS Appl Mater Interfaces* **7**(32): 18136–18144 (2015).

[17] Khadem, M, Penkov, O V, Jais, J, Bae, S-M, Dhandapani, V S, Kang, B, Kim, D-E. Formation of discrete periodic nanolayered coatings through tailoring of nanointerfaces—Toward zero macroscale wear. *Sci Adv* **7**(47): eabk1224 (2021).

[18] Ma, L, Nemati, N, Kim, D-E, Aghababaei, R. Interface Amorphization Controls Maximum

Wear Resistance of Multinanolayer DLC/WC Coatings. *ACS Appl Mater Interfaces* **16**(14): 18090–18098 (2024).

[19] Nemati, N, Penkov, O V, Kim, D-E. Superior surface protection governed by optimized interface characteristics in WC/DLC multilayer coating. *Surf Coat Technol* **385**: 125446 (2020).

[20] Li, X, Lan, Y, Jia, Q, Lv, J, Zhang, B. Dynamic gas modulation in HiPIMS architectures graded a-C:Ti/a-C:Ti:N nanolaminates for Ti bipolar plates. *J Power Sources* **673**: 239751 (2026).

[21] Xing, Z, Wang, X, Wang, X, Xu, C, Zhang, B. Unlocking the secrets of Ti / Si co-doped diamond-like carbon films for high-performance lubrication in humid environments. *Diam Relat Mater* **156**: 112402 (2025).

[22] Wang, D, Geng, Z, Chen, L, Wang, F, Shang, L, Pan, D, Zhang, G. B/N doping and plasma etching: coupling synergistic effects on tribological properties of amorphous carbon films in methane. *Appl Surf Sci* **720**: 165213 (2026).

[23] Li, M, Liu, Y, Kim, D-E, Penkov, O V. Graphene tribofilm formation on hydrogen-free DLC/B4C periodical nano-multilayer coatings: Effect of sputtering in N2 atmosphere. *Carbon* **243**: 120529 (2025).

[24] Thompson, A P, Aktulga, H M, Berger, R, Bolintineanu, D S, Brown, W M, Crozier, P S, In 'T Veld, P J, Kohlmeyer, A, Moore, S G, Nguyen, T D, Shan, R, Stevens, M J, Tranchida, J, Trott, C, Plimpton, S J. LAMMPS - a flexible simulation tool for particle-based materials modeling at the atomic, meso, and continuum scales. *Comput Phys Commun* **271**: 108171 (2022).

[25] Wu, P, Ding, X, Hu, H, Penkov, O V. Molecular Dynamics Simulation of Deposition and

Nanoindentation in SiN_x /BN_y Amorphous Periodical Nanolayered Coatings: Insights into Growth and Strengthening Mechanisms. *ACS Appl Nano Mater* **8**(22): 11495–11507 (2025).

[26] Matsunaga, K, Fisher, C, Matsubara, H. Tersoff Potential Parameters for Simulating Cubic Boron Carbonitrides. *Jpn J Appl Phys* **39**(1A): L48 (2000).

[27] Matsunaga, K, Iwamoto, Y. Molecular Dynamics Study of Atomic Structure and Diffusion Behavior in Amorphous Silicon Nitride Containing Boron. *J Am Ceram Soc* **84**(10): 2213–2219 (2001).

[28] Tersoff, J. Modeling solid-state chemistry: Interatomic potentials for multicomponent systems. *Phys Rev B* **39**(8): 5566–5568 (1989).

[29] Stukowski, A. Visualization and analysis of atomistic simulation data with OVITO–the Open Visualization Tool. *Model Simul Mater Sci Eng* **18**(1): 015012 (2010).

[30] Cao, X, Shang, L, Liang, Y, Zhang, G, Lu, Z, Xue, Q. The Tribological Performances of the Boron Carbide Films Tested under Wet Air and Wet N2 Conditions. *Tribol Lett* **67**(3): 70 (2019).

[31] He, Z, Shi, P, Zhong, X, Zhang, H, Zhuo, P, Li, J, Chen, X, Qian, L, Wang, Y. Friction condition switching two-type transfer layers of hydrogenated amorphous carbon with distinct tribological behaviors. *Carbon* **238**: 120198 (2025).

[32] Li, M, Liu, Y, Kim, D-E, Penkov, O V. Enhanced mechanical and tribological performance of W/B4C periodic nano-multilayer coating by optimizing W deposition power. *Thin Solid Films* **825**: 140716 (2025).

[33] Bhowmick, S, Sun, G, Alpas, A T. Low friction behaviour of boron carbide coatings (B4C) sliding against Ti–6Al–4V. *Surf Coat Technol* **308**: 316–327 (2016).

[34] He, D, Zhao, Y, Li, W, Shang, L, Wang, L, Zhang, G. Superior mechanical and tribological properties governed by optimized modulation ratio in WC/a-C nano-multilayers. *Ceram Int* **47**(12): 16861–16869 (2021).

[35] Ferrari, A C, Meyer, J C, Scardaci, V, Casiraghi, C, Lazzeri, M, Mauri, F, Piscanec, S, Jiang, D, Novoselov, K S, Roth, S, Geim, A K. Raman Spectrum of Graphene and Graphene Layers. *Phys Rev Lett* **97**(18): 187401 (2006).

[36] Ferrari, A C. Determination of bonding in diamond-like carbon by Raman spectroscopy. *Diam Relat Mater* **11**(3): 1053–1061 (2002).

[37] Won, M-S, Penkov, O V, Kim, D-E. Durability and degradation mechanism of graphene coatings deposited on Cu substrates under dry contact sliding. *Carbon* **54**: 472–481 (2013).

[38] Min, Y, Penkov, O V, Khadem, M, Kim, D-E. Effects of molybdenum-based substrate coatings on tribological performance of graphene films. *Carbon* **176**: 488–499 (2021).

[39] Berman, D, Deshmukh, S A, Sankaranarayanan, S K R S, Erdemir, A, Sumant, A V. Extraordinary Macroscale Wear Resistance of One Atom Thick Graphene Layer. *Adv Funct Mater* **24**(42): 6640–6646 (2014).

[40] Liu, Y, Fan, Z, Yu, S, Zhang, R, Zhang, J, Liskiewicz, T W, Ge, X, Wang, W. Macroscale structural superlubricity: Dynamic evolution of tribolayers in two-dimensional materials under extreme pressure. *Nano Energy* **129**: 110072 (2024).

[41] Piazza, F, Monthioux, M, Puech, P, Gerber, I C. Towards a better understanding of the structure of diamanoïds and diamanoïd/graphene hybrids. *Carbon* **156**: 234–241 (2020).

[42] Wang, J, Cao, X, Lu, Z, Zhang, G, Xue, Q. The improved mechanical and tribological properties of amorphous carbon film by doping boron carbide. *Ceram Int* **46**(7): 9878–9884

(2020).

[43] Shao, Q, Wang, S, Yuan, M, Wang, H, Jung, J C-Y, Zhang, J. Advanced boron-doped carbon papers with excellent electrical conductivity and low graphitization temperature for PEM fuel cells. *Int J Hydrog Energy* **50**: 1279–1293 (2024).

[44] Wang, X, Liu, B, Xiao, X, Wang, S, Huang, W. Boron dopant simultaneously achieving nanostructure control and electronic structure tuning of graphitic carbon nitride with enhanced photocatalytic activity. *J Mater Chem C* **9**(41): 14876–14884 (2021).

[45] Jia, Q, Yang, Z, Sun, L, Gao, K, Zhang, B, Zhang, X, Zhang, J. Catalytic superlubricity via in-situ formation of graphene during sliding friction on Au@a-C:H films. *Carbon* **186**: 180–192 (2022).

[46] Liu, Y, Li, J, Ge, X, Yi, S, Wang, H, Liu, Y, Luo, J. Macroscale Superlubricity Achieved on the Hydrophobic Graphene Coating with Glycerol. *ACS Appl Mater Interfaces* **12**(16): 18859–18869 (2020).

[47] Jin, B, Chen, G, He, Y, Zhang, C, Luo, J. Lubrication properties of graphene under harsh working conditions. *Mater Today Adv* **18**: 100369 (2023).

[48] Wang, H, Xiao, H, Lu, Y, Jiang, J. The catalytic effect of boron nitride on the mechanical properties of polyacrylonitrile-based carbon fiber. *J Mater Sci* **51**(24): 10690–10700 (2016).

[49] Lee, S, Cho, S Y, Chung, Y S, Choi, Y C, Lee, S. High electrical and thermal conductivities of a PAN-based carbon fiber via boron-assisted catalytic graphitization. *Carbon* **199**: 70–79 (2022).

[50] Ferrari, A C, Robertson, J. Interpretation of Raman spectra of disordered and amorphous carbon. *Phys Rev B* **61**(20): 14095–14107 (2000).

[51] Kong, C, Guo, P, Sun, L, Zhou, Y, Liang, Y, Li, X, Ke, P, Lee, K-R, Wang, A. Tribological mechanism of diamond-like carbon films induced by Ti/Al co-doping. *Surf Coat Technol* **342**: 167–177 (2018).

[52] Chen, Q, Xu, X, Li, A, Zhang, Q, Yang, H, Qiu, N, Wang, Y. Fretting wear resistance of amorphous/amorphous (AlCrFeNi)N/TiN high entropy nitride nanolaminates. *J Mater Sci Technol* **182**: 41–53 (2024).

[53] Penkov, O V, Khadem, M, Lee, J-S, Kheradmandfard, M, Kim, C-L, Cho, S-W, Kim, D-E. Highly durable and biocompatible periodical Si/DLC nanocomposite coatings. *Nanoscale* **10**(10): 4852–4860 (2018).

[54] Wu, P, Uzoma, P C, Li, M, Kim, D-E, Penkov, O V. Atomistic insights into architecture-dependent friction and deformation in SiNx/BNy amorphous periodic nanolayered coatings. *Appl Surf Sci* **741**: 167180 (2026).

[55] Doan, D-Q, Vu, H-C, Nguyen, V-T, Vu, T-Q, Tran, V-T, Chu, V-T. An atomic-scale insight into mechanical enhancement and frictional properties of amorphous/graphene multilayers. *Tribol Int* **197**: 109783 (2024).

[56] Zhou, Q, Luo, D, Hua, D, Ye, W, Li, S, Zou, Q, Chen, Z, Wang, H. Design and characterization of metallic glass/graphene multilayer with excellent nanowear properties. *Friction* **10**(11): 1913–1926 (2022).

[57] Ye, Y X, Liu, C Z, Wang, H, Nieh, T G. Friction and wear behavior of a single-phase equiatomic TiZrHfNb high-entropy alloy studied using a nanoscratch technique. *Acta Mater* **147**: 78–89 (2018).

[58] Zhu, X, Wang, X, Liu, Y, Luo, Y, Liu, Y, Zhang, H, Zhao, X. Effect of the Graphitization

Mechanism on the Friction and Wear Behavior of DLC Films Based on Molecular Dynamics Simulations. *Langmuir* **39**(5): 1905–1913 (2023).

[59] Baral, P, Jaddi, S, Wang, H, Orekhov, A, Gauquelin, N, Bagherpour, A, Van Loock, F, Coulombier, M, Favache, A, Rusinowicz, M, Verbeeck, J, Lucas, S, Raskin, J-P, Idrissi, H, Pardoen, T. Al2O3/Al hybrid nanolaminates with superior toughness, strength and ductility. *Nat Commun* **16**(1): 1355 (2025).

Mingfeng Li. He is currently a Ph.D. student in the School of Mechanical Engineering at Zhejiang University and the Zhejiang University-University of Illinois Urbana-Champaign Institute (ZJU-UIUC Institute). His research interests center on X-ray characterization of periodic nanomultilayer coatings and their applications in diverse fields, particularly tribology and optics.

Pengyuan Wu. He is currently a Ph.D. student in the School of Materials Engineering at Zhejiang University and the Zhejiang University-University of Illinois Urbana-Champaign Institute (ZJU-UIUC Institute). He concentrates on

SiNx/BN nanolayer periodic structure with excellent mechanical durability, sapphire-level hardness, optical transparency, and flexibility.

Boyang Shen. He is currently pursuing a Ph.D. degree at the School of Mechanical Engineering, Zhejiang University. His research focuses on the development and characterization of biocompatible diamond-like carbon (DLC) based coatings fabricated via magnetron sputtering technology for biomedical applications.

Dae-Eun Kim. He is currently a Full Professor at the School of Mechanical Engineering, Yonsei University, Republic of Korea. Professor KIM received his Ph.D. degree in Mechanical Engineering from Massachusetts Institute of Technology (MIT), USA. Professor KIM served as the President of the Korean Society for Precision Engineering and the President of the Korean Tribology Society. Professor KIM is a Fellow of the International Academy for Production Engineering (CIRP) and a Fellow of the Korean Academy of Science and Technology. His research interests are tribology, coatings and surface modification.

 Oleksiy V. Penkov. He is currently a Tenured associate professor at the Zhejiang University - University of Illinois Urbana-Champaign Institute (ZJU-UIUC Institute), an adjunct associate professor at the University of Illinois Urbana-Champaign, and the head of Cross-Scale Materials Innovation Center. In 2007, he received his doctorate degree in physics and mathematics, specializing in solid-state physics from the National Technical University "KhPI" (Ukraine). During 2011–2019, he was a research professor at the Center for Nano-Wear at Yonsei University (Korea). He has been working in the field of nanomaterials and coatings. He has over 25 years of experience developing periodic nanolayered structures for various applications.